Hydrodechlorination of 4-chlorophenol on Pd–Cu/activated carbon bimetallic catalysts

Xu Fang[a], Jinbo Zhao[a], Deren Fang[a,b],*

[a]*Institute of Applied Catalysis, Yantai University, Yantai 264005, China, emails: fdr@ytu.edu.cn (D. Fang), 164196917@qq.com (X. Fang), shenyenicai@163.com (J. Zhao)*
[b]*Light Hydrocarbon Comprehensive Utilization Engineering Center, Yantai University, Yantai 264005, China*

ABSTRACT

In this study, a series of activated carbon (AC)-supported Pd–Cu bimetallic catalysts were prepared using the sequential incipient wetness impregnation method, and another series of nonsupported Pd–Cu bimetallic catalysts was prepared using the reversed-phase microemulsion method. The performance of these catalysts in the hydrodechlorination (HDC) of 4-chlorophenol (4-CP) was investigated. The catalysts were characterised using temperature-programmed reduction, X-ray diffraction, X-ray photoelectron spectroscopy, high-resolution transmission electron microscopy (HRTEM), and scanning electron microscopy–energy-dispersive X-ray spectroscopy (SEM–EDS). The results demonstrated that the Pd–Cu/AC catalysts achieved fast conversion of 4-CP and exhibited high selectivity for phenol and that Pd was the active centre for the HDC reaction of 4-CP. For low Cu content, the main function of Cu was to separate the Pd particles to prevent them from growing; when the Cu content exceeded a certain threshold, the catalytic activity decreased. Specifically, the catalytic activity of the catalysts decreased when the Pd particles were doped with Cu. HRTEM and SEM–EDS demonstrated that a Cu–Pd alloy formed in the nonsupported Pd–Cu catalysts and that these catalysts exhibited lower catalytic activity in the HDC of 4-CP than the supported Pd–Cu/AC bimetallic catalysts. The formation of a Cu–Pd alloy was not conducive to the HDC reaction. The results indicated that the active centre for the formation of cyclohexanone may be point or line defects on the edge of Pd particle junctions with the carrier. The HDC reaction of 4-CP is a structure-sensitive reaction.

Keywords: Pd–Cu/AC bimetallic catalyst; Hydrodechlorination; Cu–Pd alloy; 4-Chlorophenol

1. Introduction

Chlorophenols (CPs) generally exhibit high toxicity and poor biodegradability and can have adverse effects on the environment and humans, despite their widespread use as end products or intermediates in pesticides, disinfectants, wood preservatives, and personal care formulations [1,2]. Therefore, the investigation of environmentally safe methods of CP disposal is a critical field of research. Conventional destructive techniques—such as biological [3], thermal [4], and chemical techniques [5]—of treating CP waste streams have limited applicability [6]. Hydrodechlorination (HDC)

may be a potential solution because it is a clean, relatively inexpensive, and efficient technique that can be used under mild conditions; moreover, it substantially reduces the toxicity of CP waste streams and is effective for a wide range of CP concentrations [7,8].

Studies on the catalytic HDC of CPs in aqueous solutions have mainly focused on single noble metal supported catalysts such as Pd [6,9–12,14–17], Pt [6,18,19], and Rh [6,16,20,21]. Among these metals, Pd is the most active and selective catalyst. Recently, Pd–M bimetallic catalysts such Pd–Cu/Al$_2$O$_3$ [22], Pd–In/Al$_2$O$_3$ [23], Pd–Bi/Al$_2$O$_3$ [24],

* Corresponding author.

Pd–Bi/SiO$_2$ [24], and Pd–Fe/Al$_2$O$_3$ [25] have drawn greater attention and shown higher activity in liquid-phase HDC than other catalysts [26]. Numerous researchers have concluded that HDC is a structure-sensitive reaction and that the catalyst carrier plays a crucial role in the reaction [16,27–29]. Through conducting an experiment, De Pedro et al. [30] concluded that a Pd/activated carbon (AC) catalyst maintains constant activity at a considerably higher rate compared with the residual activity of a Pd/Al$_2$O$_3$ catalyst. Dong et al. [13] discovered that a novel fibrous nanosilica-based nanocatalyst used in the catalytic reduction HDC of 4-chlorophenol (4-CP) had a dandelion-like shape, high surface area, and easily accessible active sites. Furthermore, he found that Ni metal–organic framework–derived N-doped magnetic mesoporous carbon-supported Pd nanoparticle catalysts exhibited high catalytic stability and recyclability in the catalytic reduction HDC of 4-CP [31]. Other studies have demonstrated that the catalytic performance of supported noble metal catalysts is affected by the size and structure of the metal particles [16,25,27,32,33]. Karanjit et al. [34] found that the stabilisation effect of Au on Pd changed the reactivity of the Pd in Au/Pd bimetallic nanoclusters, altering the reaction mechanism from homogeneous to heterogeneous in the HDC of aryl chlorides. Zhou et al. [35] also discovered that bimetallic catalysts had smaller metal particles and more exposed active sites than monometallic catalysts.

We previously investigated the catalytic activity of Pd–Cu/Al$_2$O$_3$ and Pd–In/Al$_2$O$_3$ bimetallic catalysts in the HDC of 4-CP in an aqueous phase and found that the addition of a small quantity of Cu or In improved the catalytic activity of Pd/Al$_2$O$_3$ [22,23]. The AC-supported palladium–copper bimetallic catalyst was confirmed to have the highest catalytic activity using a denitrification experiment [36]. The performance of AC-supported Pd–Cu/AC bimetallic catalysts in the HDC of 4-CP in the aqueous phase has not yet been reported, nor the effect mechanism of Cu towards Pd has been studied. In the present paper, we describe the performance of bimetallic catalysts Pd–Cu/AC in the HDC of 4-CP in the aqueous phase. The reaction rates of some Pd–Cu/AC catalysts were found to be higher than those of Pd–Cu/Al$_2$O$_3$ catalysts, and these Pd–Cu/AC catalysts also have higher phenol selectivity. This is because the AC support promotes the catalytic activity and restrains tandem reaction. A preliminary study was also performed to investigate the effect mechanism of Cu towards Pd in the catalysts. To the best of our knowledge, these results have not been reported by other studies and clarify this situation.

2. Experimental

2.1. Catalyst preparation

The method for preparing Pd–Cu/AC bimetallic catalysts was adopted from a previous study [23]. The Pd content was fixed at 1 wt%, and the Cu content was varied to obtain Cu/Pd molar ratios of 0.1/1, 0.3/1, 0.5/1, 1/1, and 3/1. The corresponding catalysts were designated as CuPd-0.1/1, CuPd-0.3/1, CuPd-0.5/1, CuPd-1/1, and CuPd-3/1, respectively.

The nonsupported Pd–Cu bimetallic catalysts were prepared using the reversed-phase microemulsion method. Reverse microemulsion was prepared through mixing 50 mL of cyclohexane, 30 mL of isopropanol, and 3 g of dodecyl

sodium sulphate in a flask. The same mixture was prepared in two separate flasks. The reverse microemulsion (water-in-oil) was vigorously magnetic stirred at 30°C for 2 h [37]. Subsequently, the designated amount of aqueous PdCl$_2$ and aqueous Cu(NO)$_3$ was added to one flask and magnetically stirred for 0.5 h. Under identical conditions, the designated amount of aqueous NaBH$_4$ was added to another flask. The two flasks were then mixed together rapidly. After 2 h of stirring, the compound was filtered and washed several times with deionised water to remove residual surfactants and organic solvents. Similarly to the supported catalysts, the Pd content was fixed at 1 wt% and the Cu content was varied to obtain Cu/Pd molar ratios of 0.1/1, 0.3/1, 0.5/1, 1/1, and 3/1; the corresponding catalysts were designated as CuPd(me)-0.1/1, CuPd(me)-0.3/1, CuPd(me)-0.5/1, CuPd(me)-1/1, and CuPd(me)-3/1, respectively.

2.2. Catalytic HDC

HDC of 4-CP was performed at atmospheric pressure in a mixing glass tank reactor with electromagnetic stirring to ensure full contact between the catalyst and reactant. After reduction, 0.2 g of the catalyst was added to a 400 mL aqueous mixture of 4-CP (1,000 ppm) and NaOH (NaOH/4-CP molar ratio was 1.1/1). Subsequently, H$_2$ was introduced into the reactor at a rate of 50 mL min^{-1}, thus initiating the HDC. After the reaction, 1 mL of the solution was extracted at defined intervals and analysed using gas chromatography with a flame ionisation detector and a polyethylene glycol capillary column.

2.3. Catalyst characterisation

X-ray diffraction (XRD) patterns of the solid products were obtained using a Shimadzu XRD-6100 X-ray diffractometer (Cu Kα radiation) equipped with a computer system for automatic operation and data processing [22].

X-ray photoelectron spectroscopy (XPS) was performed using a PHI 5000 VersaProbe spectrometer equipped with a high-performance Al monochromatic source. XPS spectra were referenced to the C1s peak at 284.6 eV.

High-resolution transmission electron microscopy (HRTEM) images were obtained using a JEM-200CX electron microscope equipped with a computer system for automatic operation and data processing. The particle morphologies of Pd and Cu were also determined using HRTEM. HRTEM images were analysed using the software Digital Micrograph Demo [38].

Temperature-programmed reduction (TPR) was performed using a TP5000 multifunction absorber [22].

H$_2$–O$_2$ pulse chemisorption measurements of the catalysts were also performed using the TP5000 multifunction absorber and a thermal conductivity detector [23]. The Pd surface areas and dispersions of the catalysts are listed in Table 1.

Scanning electron microscopy (SEM) images were obtained using a Hitachi S-4800 field-emission scanning electron microscope equipped with a computer system for automatic operation and data processing. A dried sample was carefully transferred to a carbon tape on the SEM template, coated using a gold coater, and analysed at 10 kV.

Energy-dispersive X-ray (EDX) experiments were performed using an EX-350 EDX microanalyser equipped with a computer system for automatic operation and data processing. EDX mapping was performed to visualise the elemental and spatial information. The particle morphology of Pd and Cu was determined through transmission electron microscopy (TEM) using a JEOL JEM2000EXII microscope.

3. Results and discussion

Fig. 1 shows the H_2-TPR profiles of the catalysts, in which 1% Pd and 1% Cu show only one reduction peak and have reduction temperatures of 355 and 476 K, respectively. The negative peak for 1% Pd at 400 K corresponds to the decomposition of Pd β-hydride.

The TPR profiles of the Pd–Cu bimetallic catalysts differ from those of the monometallic catalysts. The reduction peaks centred at 355 and 453 K were attributed to PdO and CuO, respectively. The reduction peak between PdO and CuO may be attributable to the successive reduction of PdO and CuO; PdO was first reduced to metal Pd, after which the hydrogen molecules that had adsorbed onto its surface dissociated into hydrogen atoms, which overflowed to the surface of CuO in contact with the Pd particles, forming a Pd–Cu particle, in which some type of reaction between Pd and Cu occurred. Increasing the Cu content increased the complexity of the TPR profiles. The TPR profiles of the CuPd-3/1 catalyst
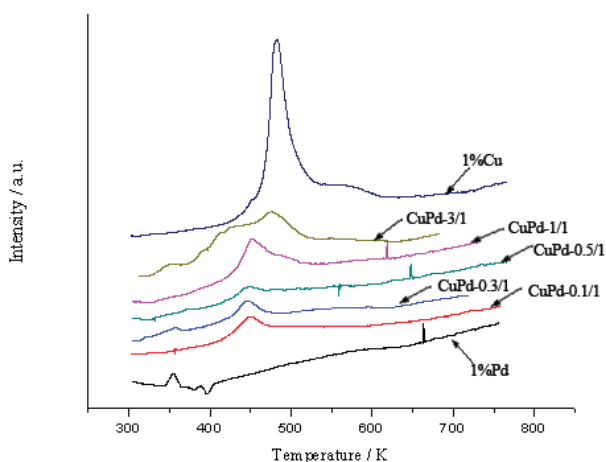
have a middle peak at approximately 412 K. The number of peaks increased with an increase in Cu content, indicating the presence of Pd–Cu particles with some Pd–Cu interaction in the catalyst. The TPR results show that as the Cu content was increased, the interaction between PdO and CuO increased and the reduction products became more diverse. The TPR profiles of the catalysts may indicate the existence of separate CuO particles and PdO particles and the overlap of some CuO particles and PdO particles in the catalyst's precursor. During the process of reduction, the former were changed to discrete Cu and Pd particles, whereas the latter were altered to a variety of intimate-contact Pd–Cu particles with different compositions. Another noteworthy phenomenon was that the peak corresponding to Pd β-hydride decomposition was absent in the profiles of all Pd–Cu bimetallic catalyst samples, which may indicate that the presence of Cu altered the crystal structure of Pd particles, making the generation of Pd β-hydride unfavourable. This is also explained from the conclusion that interaction between Pd and Cu did occur.

Fig. 2 presents the XRD patterns of the catalysts. Diffraction peaks corresponding to Pd at 2θ values of 40.1°, 46.6°, and 68.1° were expected for the Pd–Cu/AC catalysts. The figure shows that the intensity of the Pd peaks gradually decreases with an increase in Cu content, indicating that increasing the Cu content caused the Pd surface to become covered by Cu, forming Pd–Cu particles with some structural differences from pure metal Pd [22]. Additionally, with an increase in Cu content, the peak intensity at a 2θ value of 44.5° gradually increased. We speculate that this peak corresponds to Cu–Pd particles; thus, the microstructure of these particles requires further investigation.

Table 1 lists the Pd surface area and dispersion of the catalysts that had AC as a carrier. The bimetallic catalysts with Cu/Pd molar ratios of 0.1/1, 0.3/1, and 0.5/1 (CuPd-0.1/1, CuPd-0.3/1, and CuPd-0.5/1, respectively) had higher Pd dispersion and surface areas than the 1% Pd monometallic catalyst. This was due to the presence of a small amount of copper, which isolated the Pd. However, the Pd–Cu/AC bimetallic catalysts with Cu/Pd molar ratios of 1/1 and 3/1 (CuPd-1/1 and CuPd-3/1) exhibited lower Pd dispersion and surface areas than the 1% Pd monometallic catalyst, indicating that

Table 1
Dispersion of Pd and surface area of the catalysts with AC as the carrier

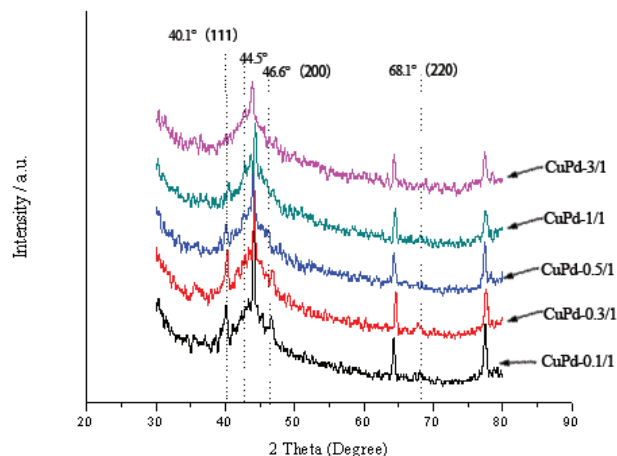| Catalysts	Molar ratios of Cu/Pd	Pd dispersion (%)	Pd surface area (m^2 g^{-1})
1%Pd	–	28.1	62.5
CuPd-0.1/1	0.1/1	35.9	80.1
CuPd-0.3/1	0.3/1	41.6	92.7
CuPd-0.5/1	0.5/1	32.4	72.2
CuPd-1/1	1.0/1	21.8	48.7
CuPd-3/1	3.0/1	14.3	31.8

Fig. 1. TPR profiles of the catalysts.

Fig. 2. XRD patterns of the reduced catalysts with various Cu–Pd molar ratios.

adding Cu altered the Pd dispersion and surface area of the bimetallic catalysts. This may be because of a large amount of copper and palladium cross-distribution in which some of the Pd surface was overlapped by Cu, resulting in Pd surface area and dispersion decreases.

The 3d Pd XPS spectra of the CuPd-0.3/1 and CuPd-3/1 catalysts (Fig. 3(a)) have two main peaks at 335.1 and 340.3 eV, which correspond to the Pd $3d_{5/2}$ and Pd $3d_{3/2}$ binding energies of Pd^0, respectively [39]. This demonstrates that adding Cu to the Pd monometallic catalyst does not change the state of metal Pd. The 2p Cu XPS spectra of the CuPd-0.3/1 and CuPd-1/1 catalysts (Fig. 3(b)) have two main peaks at 932.6 and 952.5 eV, which correspond to the Cu $2p_{3/2}$ and Cu $2p_{1/2}$ binding energies of Cu^0, respectively [40]. These results reveal the presence of metal-state Pd and Cu in the catalysts.

The HRTEM results presented in Fig. 4 indicate that the Pd particle sizes of the catalysts were in the range of 1–6 nm and Fig. S1 indicates that the mean particle sizes of the CuPd-0.3/1, CuPd-0.5/1, CuPd-1/1, and CuPd-3/1 catalysts were 2.5, 3.1, 3.4, and 4.3 nm, respectively. These results demonstrate that the catalyst particle size increased with the Cu content, indicating that the Pd particles became covered by Cu particles at higher Cu contents, which increased the grain size (observed in the micrographs) and decreased the particles' catalytic activity.

TEM/EDX images (Fig. 5) demonstrate that Pd and Cu coexisted in the same microzone of CuPd-0.5/1. We can clearly distinguish Cu and Pd particles in Figs. 5(b) and (c). Moreover, the Cu and Pd were evenly distributed on the catalyst surface.

After combining the TPR, XRD, XPS, H_2 pulse chemisorption, and TEM results, we concluded that during the reduction process, CuO and PdO were reduced to metal-state Cu and Pd, and Pd and Cu particles were separately dispersed on the surface of the catalysts when the Cu/Pd molar ratio was low. The characterisation results also reveal that some Pd–Cu particles formed a special structure after the reduction when the Cu/Pd molar ratio was high, which according to the TEM micrographs explains why the Pd particles in the CP-5 catalyst were larger than those in the CuPd-0.3/1 catalyst (Fig. 6). This means that the particles observed in the TEM micrographs were not pure Pd particles but Pd–Cu particles with some range of compositions and structures. Because the Pd and Cu content were low in the catalysts, the composition and structure of the Pd–Cu particles were not easily detected. Nonetheless, we can be certain that the Pd–Cu particles were not a compound that had a fixed composition.

Fig. 6 illustrates the performance of the catalysts in the HDC reaction. The catalytic activity of the various catalysts differed considerably and was in the order of CuPd-0.3/1 > CuPd-0.1/1 > CuPd-0.5/1 > 1% Pd > CuPd-0.1/1 > CuPd-3/1 > 1% Cu. The 4-CP was completely hydrodechlorinated within 30 min. By contrast, at the Cu/Pd molar ratios of 1/1 and 3/1, the 4-CP was not completely hydrodechlorinated even after 2 h.

The graph shows that the 1% Pd/AC catalyst converted the 4-CP completely within 60 min, whereas the 1% Cu/AC catalyst converted only a small amount of the 4-CP, even after 2 h. This implies that the active centre for the HDC of 4-CP was Pd. At low Cu/Pd molar ratios, the catalytic activity of the catalysts increased with the Cu/Pd molar ratio because the presence of Cu increased the dispersion of Pd particles (Table 1). With a further increase in the Cu content, however, the HDC reaction rate gradually decreased. In particular, at the Cu/Pd molar ratio of 3/1, the reaction speed was extremely low. De Pedro et al. [30] prepared a Pd/AC catalyst that had a conversion rate of only 70%; Karanjit et al. [34] prepared a Pd/Au catalyst that had a conversion rate of only 51%.

According to gas chromatography–mass spectrometry analysis, in addition to phenol, cyclohexanone was produced in the HDC of 4-CP in the aqueous phase, indicating
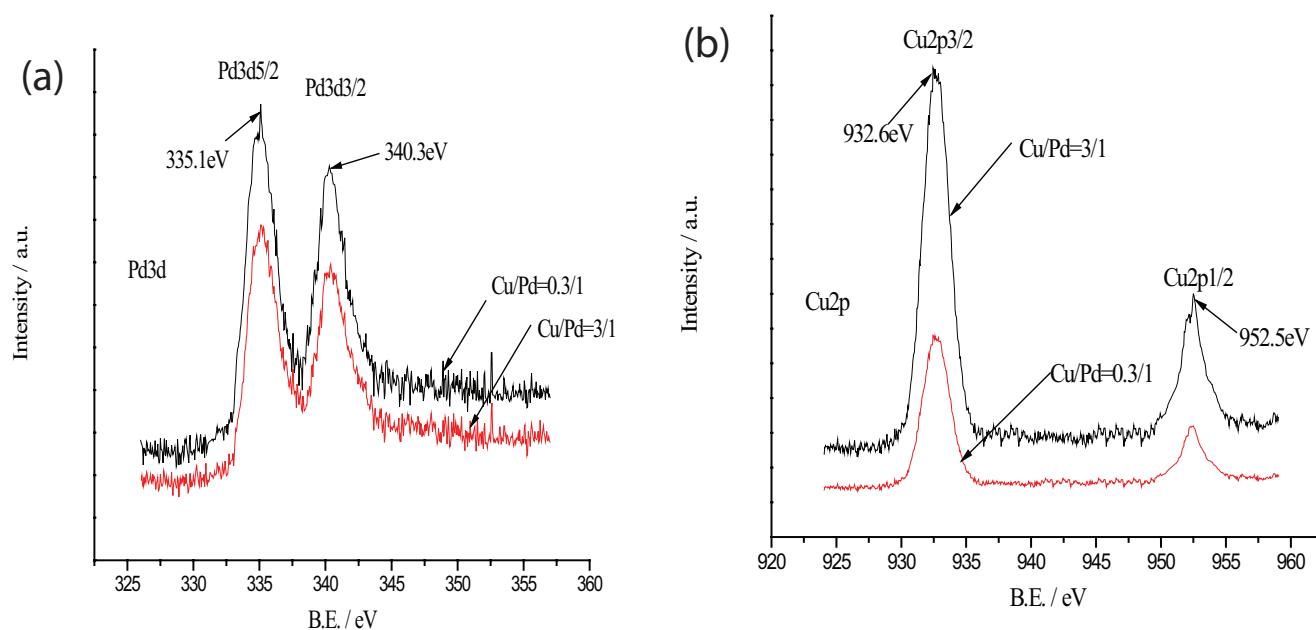

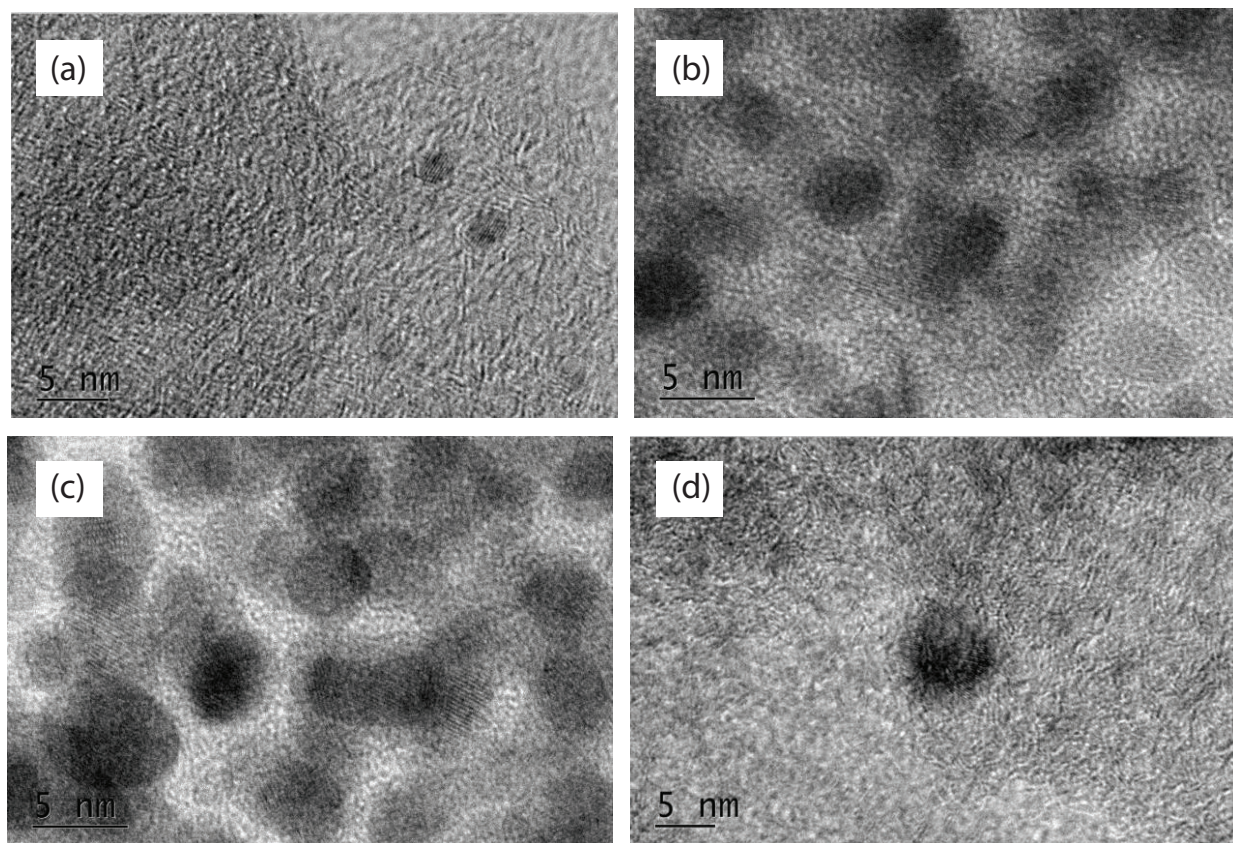Fig. 3. XPS spectra of the CuPd-0.3/1 and CuPd-3/1 catalysts: (a) Pd 3d and (b) Cu 2p.

Fig. 4. HRTEM micrographs of the reduced catalysts (a) CuPd-0.3/1; (b) CuPd-0.5/1; (c), CuPd-1/1; and (d) CuPd-3/1.
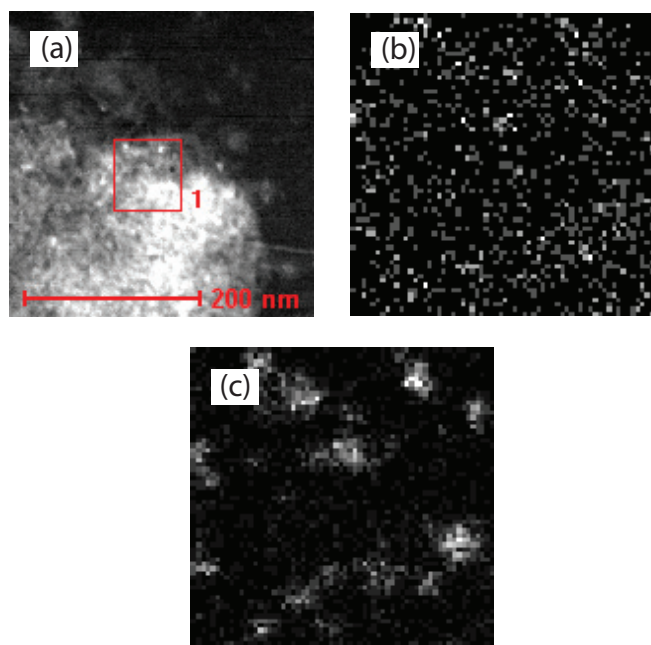

Fig. 5. TEM/EDX images of catalyst CuPd-0.5/1 (a) Cu/Pd = 0.5/1, (b) Cu Kα1 in CuPd-0.5/1, and (c) Pd Lα1 in CuPd-0.5/1.

that the HDC of 4-CP with a Cu–Pd/AC catalyst was also a tandem reaction in which the 4-CP was first hydrogenated to form phenol, which was further hydrogenated to form
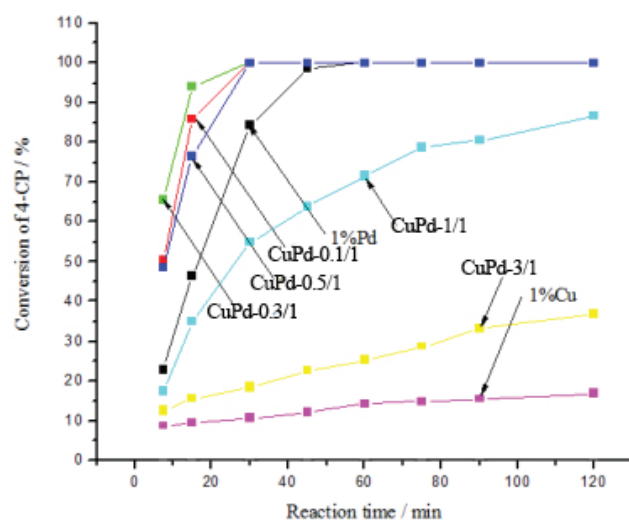

Fig. 6 Influence of catalysts composition on the conversion of 4-CP.

cyclohexanone; the reaction pathway is displayed in Fig. 7 [22,23]. Fig. 8 illustrates the variation in the selectivity of the catalysts, from which we concluded that the catalyst selectivity for PhOH was in the order of CuPd-3/1 ≈ 1% Cu > CuPd-1/1 > 1% Pd > CuPd-0.5/1 > CuPd-0.1/1 > CuPd-0.3/1, whereas the selectivity for cyclohexanone was in the reverse order. The selectivity of all the catalysts for phenol gradually decreased

with the reaction time, except for CuPd-3/1 and 1% Cu, which exhibited no activity for the production of cyclohexanone. By contrast, the selectivity of all the catalysts for cyclohexanone gradually increased with the reaction time. Fig. 6 shows that the catalytic activity of the catalysts was in the order of CuPd-0.3/1 > CuPd-0.1/1 > CuPd-0.5/1 > 1% Pd > CuPd-0.1/1 > CuPd-3/1 > 1% Cu in an aqueous solution. Competitive hydrogenation of phenol occurred during the HDC of 4-CP
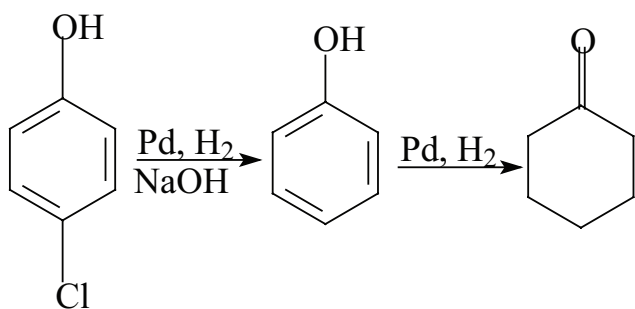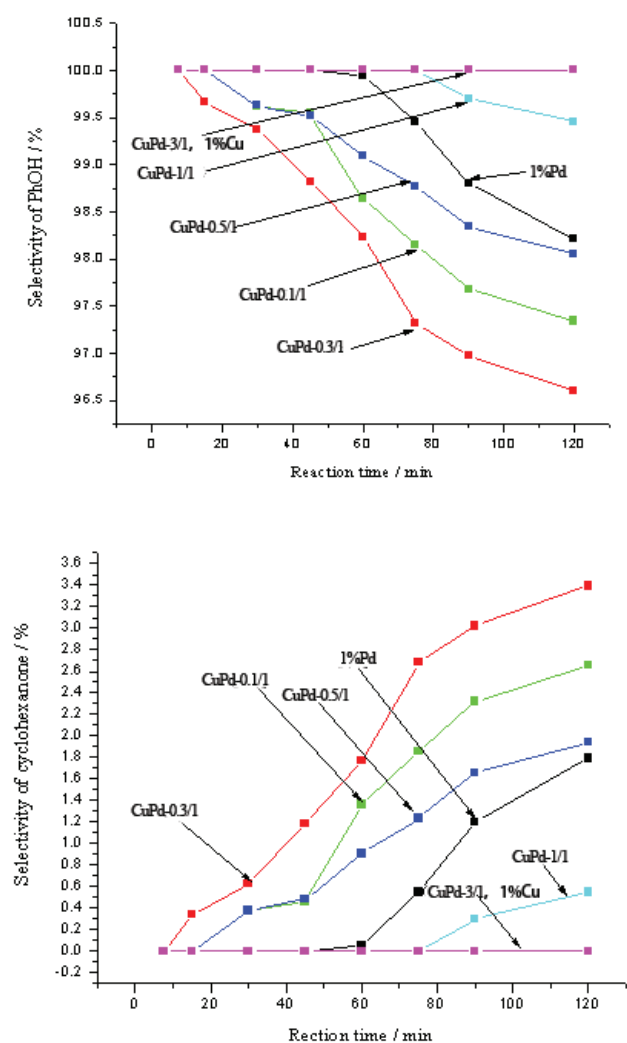

Fig. 7. The equation of the HDC of 4-CP.

over 1% Pd and using all Cu–Pd/AC bimetallic catalysts. For example, when CuPd-0.3/1 was used in the HDC of 4-CP, the 4-CP was completely hydrogenated after 30 min. The catalyst selectivity for phenol and cyclohexanone was approximately 99.3% and 0.7%, respectively, indicating that the HDC of 4-CP and the hydrogenation of phenol proceeded simultaneously over a Cu–Pd/AC bimetallic catalyst. For comparison, the Pd–In/Al$_2$O$_3$ catalyst selectivity for phenol and cyclohexanone was approximately 97.3% and 2.7%, respectively [23].

Comparing these results with those for the Cu–Pd/Al$_2$O$_3$ bimetallic catalysts [22], it was found that the Cu–Pd/AC bimetallic catalysts not only have higher catalytic activity but also higher phenol selectivity. In the case of Cu–Pd/Al$_2$O$_3$ bimetallic catalyst, the complete hydrogenation of 4-CP took at least 60 min and the selectivity of phenol was in the range of 70%–90%. The results demonstrated that in addition to catalytic activity, the carrier affected the selectivity of the reaction, indicating that the carrier might participate in the hydrogenation of phenol into cyclohexanone.

By combining the results of the catalyst characterisation and the HDC reaction, we concluded that for lower Cu/Pd molar ratios, Cu and Pd particles mostly existed in separate states, forming small Pd particles and the catalytic activity increasing as the ratio was increased; in the case of higher Cu/Pd molar ratios, however, Cu and Pd particles overlapped and Cu covered the surface of Pd, forming Pd–Cu particles with a special sketch map (Fig. 9). This reduced the surface area of the Pd and thus reduced the catalytic activity of the catalyst.
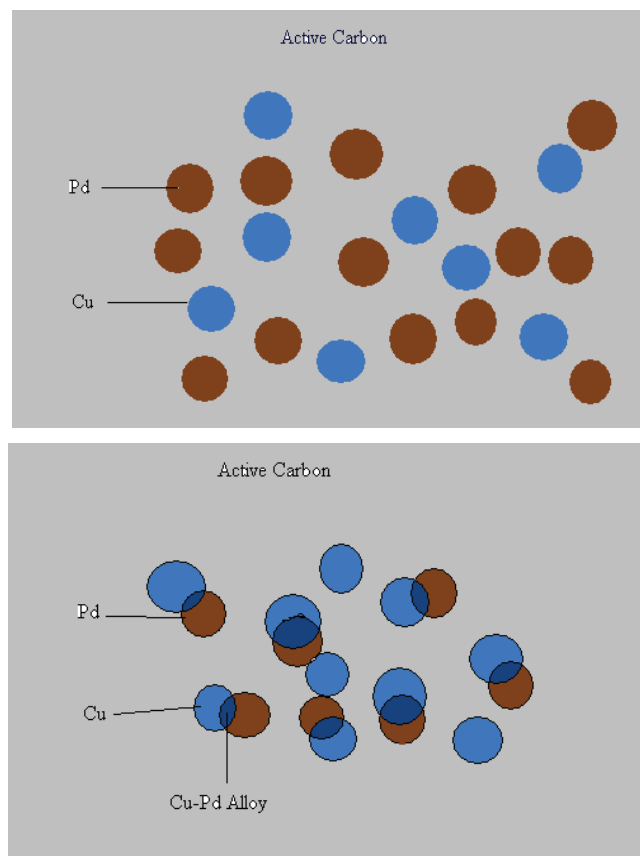

Fig. 9. Structure of the atomic arrangement.

Fig. 8. Influence of the catalysts on the hydrogenation products.

To further study the coexisting state of Cu and Pd in the catalysts, as well as the modulation mechanism of Cu on the Pd catalyst, we prepared a series of nonsupported Pd–Cu bimetallic catalysts using the reversed-phase microemulsion method and tested their catalytic activity for the HDC of the 4-CP (Fig. 7). The morphological and microarea compositions were simultaneously characterised using HRTEM (Fig. 11) and SEM–EDS (Fig. 12) to further confirm the Cu–Pd interaction in the catalysts.

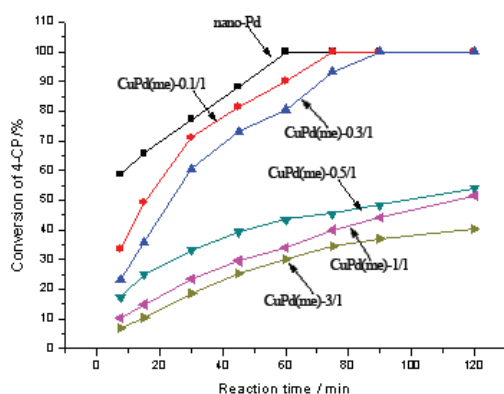Fig. 10 illustrates the performance of the nonsupported catalysts in the HDC reaction of 4-CP. The catalytic activity was in the order of nano-Pd > CuPd(me)-0.1/1 > CuPd(me)-0.3/1 > CuPd(me)-0.5/1 > CuPd(me)-1/1 > CuPd(me)-3/1. Thus, the catalytic activity of the nonsupported Pd–Cu bimetallic catalysts decreased monotonously with increasing Cu content. Furthermore, the catalytic activity of the nonsupported Pd–Cu bimetallic catalysts was lower than that of the supported Cu–Pd/AC bimetallic catalysts with the same composition. Another crucial phenomenon observed for the nonsupported Pd–Cu bimetallic catalysts was that the only hydrogenated product was phenol; no cyclohexanone was detected. These results differ from the HDC reaction of 4-CP with Cu–Pd/AC catalysts; the hydrogenation of phenol into cyclohexanone may thus have occurred at point or line defects on the edge of Pd particle junctions with the carrier. Because AC is comparatively inert, its interaction with metals is weak. To examine the influence of the carrier on the HDC reaction, pure AC was used as the catalyst for the reaction, with the remainder of the procedure kept the same. After 8 h of stirring, no phenol or cyclohexanone was detected, indicating that the AC carrier did not catalyse the HDC reaction of 4-CP. Therefore, we speculate that the further hydrogenated reaction of phenol occurs at the border of Pd particle edges with the carrier.

The HRTEM results in Fig. 11 indicate that the particle sizes of the catalysts were in the range of 2–5 nm and Fig. S2 indicates that the mean particle sizes of the CuPd(me)-0.5/1, CuPd(me)-1/1, and CuPd(me)-3/1 catalysts were 2.8, 3.0, and 3.3 nm, respectively. These results demonstrate that the catalyst particle size increased with the Cu content. Comparing Figs. 4 and 11, the metal particles in the nonsupported Pd–Cu

Fig. 10. Influence of catalysts composition on the conversion of 4-CP.
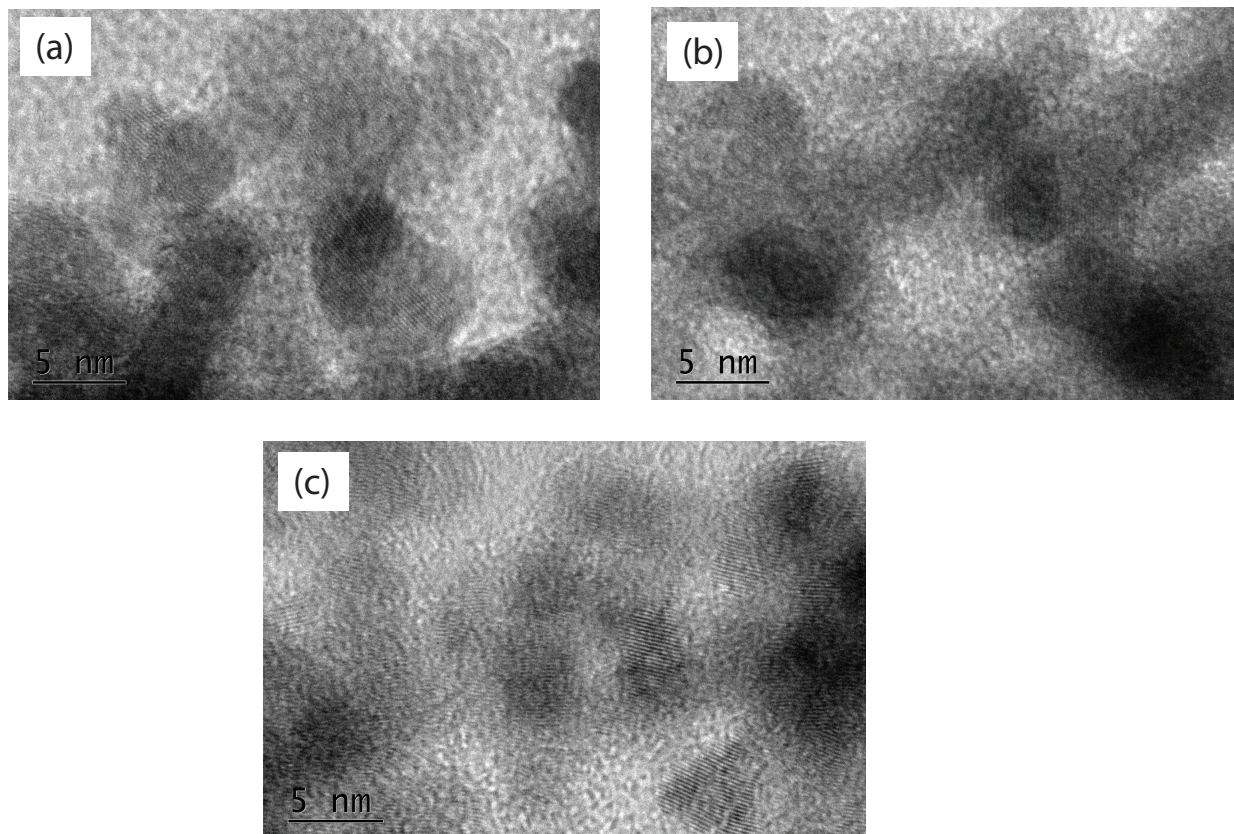

Fig. 11. HRTEM micrographs of the reduced catalysts (a) CuPd(me)-0.5/1; (b) CuPd(me)-1/1; and (c) CuPd(me)-3/1.

bimetallic catalyst were smaller than those in the supported Cu–Pd/AC catalysts. However, the catalytic activity of a supported Cu–Pd/AC catalyst was more favourable than that of the nonsupported Pd–Cu bimetallic catalyst with the same composition. This further demonstrates that microarea composition and phase structure were critical to the reaction.

The SEM–EDS results in Fig. 12 indicate that the Cu and Pd in the nonsupported Cu–Pd bimetallic catalysts were evenly distributed according to the molar ratio. The lattice plane spacing of different samples is listed in Table 2. For CuPd(me)-0.5/1 and CuPd(me)-1/1, the lattice plane spacing was defined as the distance between the (022) crystal face of Cu and (022) crystal face of Pd; for CuPd(me)-3/1, the lattice plane spacing was defined as the distance between the (002) crystal face of Cu and (002) crystal face of Pd. The results

presented in Table 2 prove that a Cu–Pd alloy was formed in the nonsupported Cu–Pd bimetallic catalyst. Fig. 13 illustrates the structure of the Cu–Pd alloy; by combining this with the catalytic activity results, we conclude that the formation of the Cu–Pd alloy is unfavourable to the HDC reaction of 4-CP. When the molar ratio of Cu and Pd is relatively low, less Cu–Pd alloy forms and more Pd is exposed, resulting in higher catalytic activity. When the Cu content is increased, more Cu–Pd alloy is formed in the catalyst, which causes a decrease in the number of active Pd sites and thus inhibits the catalytic activity. Based on this conclusion, explaining the effect of Cu on Pd in the case of the supported Cu–Pd bimetallic catalyst is not difficult: when the Cu content is low, the main function of Cu is to separate the Pd particles and produce large amounts of fine Pd particles, which have a larger
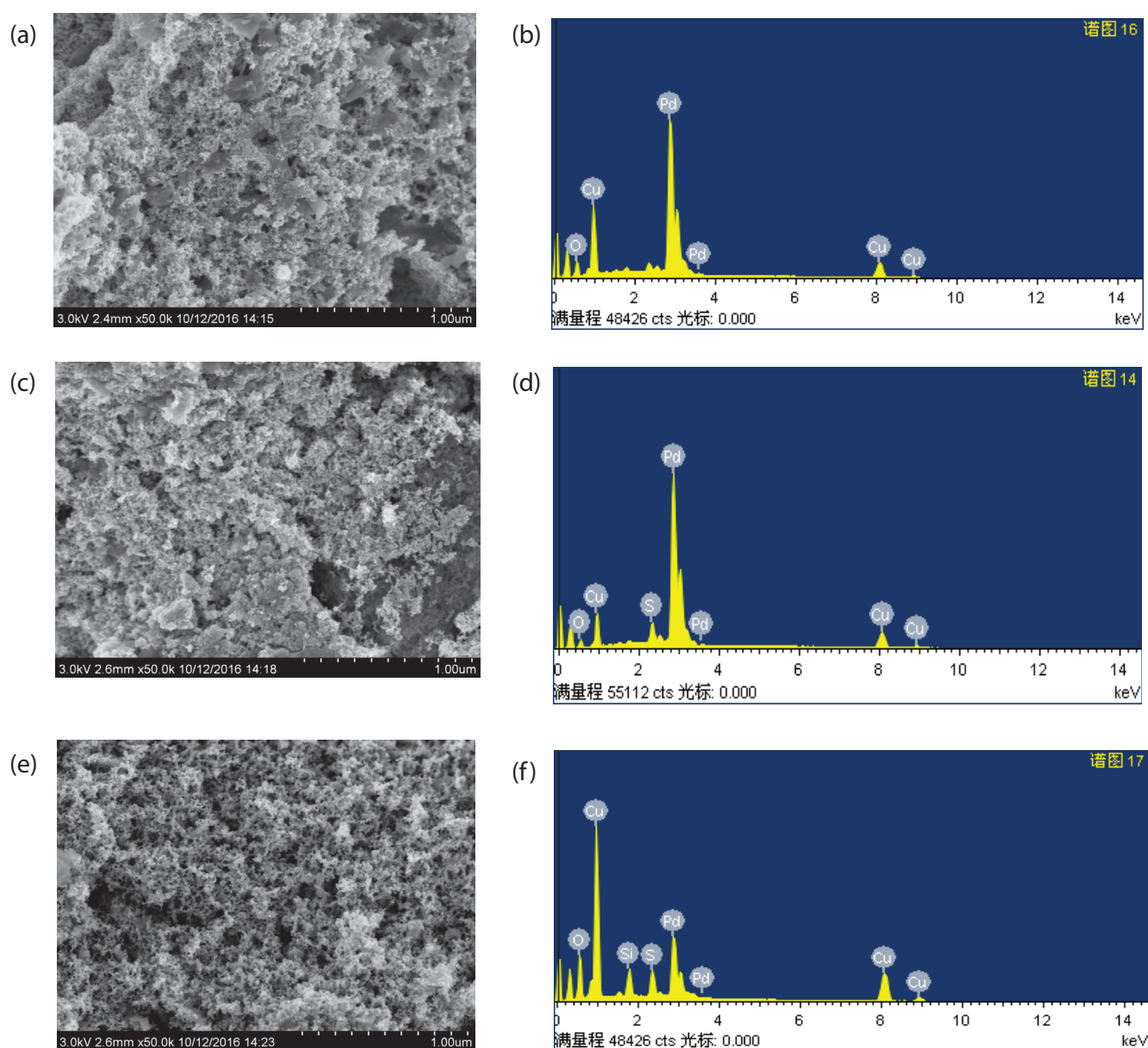

Fig. 12. SEM–EDS results for the reduced catalyst CuPd(me)-0.5/1, CuPd(me)-1/1, and CuPd(me)-3/1: (a) and (b) CuPd(me)-0.5/1; (c) and (d) CuPd(me)-1/1; and (e) and (f) CuPd(me)-3/1.

Table 2
Lattice plane spacing of catalysts with different molar ratios

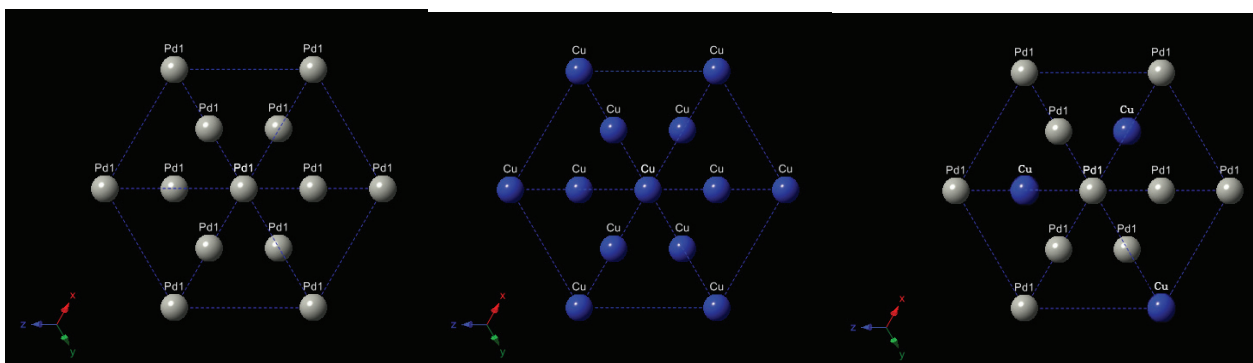| Catalysts	Molar ratios of Cu/Pd	Crystal face	Metal	Lattice plane spacing/Å
CuPd(me)-0.5/1	0.5/1	022	Pd	1.4109
			Cu	1.2664
			Cu–Pd	1.3983
CuPd(me)-1/1	1.0/1	022	Pd	1.4109
			Cu	1.2664
			Cu–Pd	1.3935
CuPd(me)-3/1	3.0/1	002	Pd	1.9954
			Cu	1.7910
			Cu–Pd	1.8246

Fig. 13. Structure of the Cu–Pd alloy.

metal surface area and thus higher catalytic activity; when the Cu content is high, some of the Cu may cover the surface of the Pd particles or form a Cu–Pd alloy, which decreases the Pd active surface area and ultimately reduces the catalytic activity. In other words, the catalytic activity of the catalysts was decreased whether or not a Pd–Cu alloy was formed in the catalysts when Cu doped Pd particles. This means that some Pd atoms participated in the formation of transition ligands during the catalytic process (i.e., the reaction mechanism involves multipoint coordination). Therefore, it is a structure-sensitive reaction [27–29].

4. Conclusion

In this study, a series of Pd–Cu/AC bimetallic catalysts were prepared, and their catalytic performance in the HDC of 4-CP in the aqueous phase was investigated. The results demonstrated that Pd was the active centre for the HDC reaction of 4-CP. In the case of low Cu content, the main function of Cu is to separate the Pd particles to prevent them from growing; when the Cu content exceeds a certain threshold, the surface of the Pd particles may be covered by Cu, a Cu–Pd alloy may be formed, or some substance with an interstitial mixture and without a fixed composition may be formed, which reduces the catalytic activity. Cu has much lower catalytic activity for the HDC reaction of 4-CP and has no catalytic activity for the generation of cyclohexanone.

A series of nonsupported Pd–Cu bimetallic catalysts were also prepared, and their catalytic performance in the HDC

of 4-CP in the aqueous phase was studied. Compared with the supported Pd–Cu/AC bimetallic catalysts, the nonsupported Pd–Cu bimetallic catalysts exhibited lower catalytic activity; furthermore, no deep hydrogenation reaction that formed cyclohexanone occurred in this system. HRTEM and SEM–EDS confirmed that the Cu–Pd bimetallic catalysts formed Cu–Pd alloys. In this reaction, the Cu–Pd alloy was not conducive to HDC reaction.

The results also demonstrated that the carrier influences the selectivity towards products and catalytic activity, indicating that the active centre for the formation of cyclohexanone may be point or line defects on the edge of Pd particle junctions with the carrier.

References

[1] M. Czaplicka, Sources and transformations of chlorophenols in the natural environment, Sci. Total Environ., 322 (2004) 21–39.
[2] E. Díaz, J.A. Casas, A.F. Mohedano, L. Calvo, M.A. Gilarranz, J.J. Rodríguez, Kinetics of the hydrodechlorination of 4-chlorophenol in water using Pd, Pt, and Rh/Al$_2$O$_3$ catalysts, Ind. Eng. Chem. Res., 47 (2008) 3840–3846.
[3] G. Moreno, G. Buitrón, Influence of the origin of the inoculum and the acclimation strategy on the degradation of 4-chlorophenol, Bioresour. Technol., 94 (2004) 215–218.
[4] P.D. Vaidya, V.V. Mahajani, Studies in hydrotreatment as a unit process to destroy 4-chlorophenol in aqueous stream over Ru-Pd/TiO$_2$ catalyst, Appl. Catal., B, 51 (2004) 21–31.
[5] G. Busca, S. Berardinelli, C. Resini, L. Arrighi, Technologies for the removal of phenol from fluid streams: a short review of recent developments, J. Hazard. Mater., 160 (2008) 265–288.

[6] C.B. Molina, A.H. Pizarro, J.A. Casas, J.J. Rodriguez, Aqueous-phase hydrodechlorination of chlorophenols with pillared clays-supported Pt, Pd and Rh catalysts, Appl. Catal., B, 148 (2014) 330–338.

[7] L. Calvo, A.F. Mohedano, J.A. Casas, M.A. Gilarranz, J.J. Rodríguez, Treatment of chlorophenols-bearing wastewaters through hydrodechlorination using Pd/activated carbon catalysts, Carbon, 42 (2004) 1377–1381.

[8] Z. Jin, C. Yu, X. Wang, Y. Wan, D. Li, G. Lu, Hydrodechlorination of chlorophenols at low temperature on a novel Pd catalyst, Chem. Commun., (2009) 4438–4440.

[9] T. Hara, T. Kaneta, K. Mori, T. Mitsudome, T. Mizugaki, K. Ebitani, K. Kaneda, Magnetically recoverable heterogeneous catalyst: palladium nanocluster supported on hydroxyapatite-encapsulated γ-Fe₂O₃ nanocrystallites for highly efficient dehalogenation with molecular hydrogen, Green Chem., 9 (2007) 1246–1251.

[10] Z. Jin, C. Yu, X. Wang, Y. Wan, D. Li, G. Lu, Liquid phase hydrodechlorination of chlorophenols at lower temperature on a novel Pd catalyst, J. Hazard. Mater., 186 (2011) 1726–1732.

[11] F.D. Kopinke, D. Angeles-Wedler, D. Fritsch, K. Mackenzie, Pd-catalyzed hydrodechlorination of chlorinated aromatics in contaminated waters—effects of surfactants, organic matter and catalyst protection by silicone coating, Appl. Catal., B, 96 (2010) 323–328.

[12] H. Rong, S. Cai, Z. Niu, Y. Li, Composition-dependent catalytic activity of bimetallic nanocrystals: AgPd-catalyzed hydrodechlorination of 4-chlorophenol, ACS Catal., 3 (2013) 1560–1563.

[13] Z. Dong, X. Le, C. Dong, W. Zhang, X. Li, J. Ma, Ni@Pd core–shell nanoparticles modified fibrous silica nanospheres as highly efficient and recoverable catalyst for reduction of 4-nitrophenol and hydrodechlorination of 4-chlorophenol, Appl. Catal., B,162 (2015) 372–380.

[14] E. Diaz, A.F. Mohedano, J.A. Casas, L. Calvo, M.A. Gilarranz, J.J. Rodriguez, Comparison of activated carbon-supported Pd and Rh catalysts for aqueous-phase hydrodechlorination, Appl. Catal., B, 106 (2011) 469–475.

[15] E. Diaz, A.F. Mohedano, J.A. Casas, L. Calvo, M.A. Gilarranz, J.J. Rodriguez, Deactivation of a Pd/AC catalyst in the hydrodechlorination of chlorinated herbicides, Catal. Today, 241 (2015) 86–91.

[16] M. Munoz, Z.M. de Pedro, J.A. Casas, J.J. Rodriguez, Improved γ-alumina-supported Pd and Rh catalysts for hydrodechlorination of chlorophenols, Appl. Catal., A,488 (2014) 78–85.

[17] H. Hildebrand, K. Mackenzie, F.D. Kopinke, Highly active Pd-on-magnetite nanocatalysts for aqueous phase hydrodechlorination reactions, Environ. Sci. Technol., 43 (2009) 3254–3259.

[18] M. Bonarowska, Z. Kaszkur, L. Kępiński, Z. Karpiński, Hydrodechlorination of tetrachloromethane on alumina- and silica-supported platinum catalysts, Appl. Catal., B, 99 (2010) 248–256.

[19] T. Yoneda, T. Takido, K. Konuma, Hydrodechlorination reactivity of para-substituted chlorobenzenes over platinum/carbon catalyst, J. Mol. Catal. A: Chem., 265 (2007) 80–89.

[20] C.B. Molina, A.H. Pizarro, M.A. Gilarranz, J.A. Casas, J.J. Rodriguez, Hydrodechlorination of 4-chlorophenol in water using Rh–Al pillared clays, Chem. Eng. J., 160 (2010) 578–585.

[21] C.S. Srikanth, V.P. Kumar, B. Viswanadham, K.V. Chary, Hydrodechlorination of 1,2,4-trichlorbenzene over supported ruthenium catalysts on various supports, Catal. Commun., 13 (2011) 69–72.

[22] D. Fang, W. Li, J. Zhao, S. Liu, X. Ma, J. Xu, C. Xia, Catalytic hydrodechlorination of 4-chlorophenol over a series of Pd-Cu/g-Al₂O₃ bimetallic catalysts, RSC Adv., 4 (2014) 59204–59210.

[23] J. Zhao, W. Li, D. Fang, Effect of indium-modified palladium catalysts on the hydrodechlorination of 4-chlorophenol, RSC Adv., 5 (2015) 42861–42868.

[24] I. Witońska, A. Królak, S. Karski, Bi modified Pd/support (SiO₂, Al₂O₃) catalysts for hydrodechlorination of 2,4-dichlorophenol, J. Mol. Catal. A: Chem., 331 (2010) 21–28.

[25] I.A. Witońska, M.J. Walock, M. Binczarski, M. Lesiak, A.V. Stanishevsky, S. Karski, Pd–Fe/SiO₂ and Pd–Fe/Al₂O₃ catalysts for selective hydrodechlorination of 2,4-dichlorophenol into phenol, J. Mol. Catal. A: Chem., 393 (2014) 248–256.

[26] F.J. Urbano, J.M. Marinas, Hydrogenolysis of organohalogen compounds over palladium supported catalysts, J. Mol. Catal. A: Chem., 173 (2001) 329–345.

[27] J.A. Baeza, L. Calvo, M.A. Gilarranz, A.F. Mohedano, J.A. Casas, J.J. Rodriguez, Catalytic behavior of size-controlled palladium nanoparticles in the hydrodechlorination of 4-chlorophenol in aqueous phase, J. Catal., 293 (2012) 85–93.

[28] G. Yuan, M.A. Keane, Role of base addition in the liquid-phase hydrodechlorination of 2,4-dichlorophenol over Pd/Al₂O₃ and Pd/C, J. Catal., 225 (2004) 510–522.

[29] G. Yuan, M.A. Keane, Catalyst deactivation during the liquid phase hydrodechlorination of 2,4-dichlorophenol over supported Pd: influence of the support, Catal. Today, 88 (2003) 27–36.

[30] Z.M. De Pedro, E. Diaz, A.F. Mohedano, J.A. Casas, J.J. Rodriguez, Compared activity and stability of Pd/Al₂O₃ and Pd/AC catalysts in 4-chlorophenol hydrodechlorination in different pH media, Appl. Catal., B, 103 (2011) 128–135.

[31] X. Cui, W. Zuo, M. Tian, Z. Dong, J. Ma, Highly efficient and recyclable Ni MOF-derived N-doped magnetic mesoporous carbon-supported palladium catalysts for the hydrodechlorination of chlorophenols, J. Mol. Catal. A: Chem., 423 (2016) 386–392.

[32] N. Yan, C. Xiao, Y. Kou, Transition metal nanoparticle catalysis in green solvents, Coord. Chem. Rev., 254 (2010) 1179–1218.

[33] J.A. Baeza, L. Calvo, M.A. Gilarranz, J.J. Rodriguez, Effect of size and oxidation state of size-controlled rhodium nanoparticles on the aqueous-phase hydrodechlorination of 4-chlorophenol, Chem. Eng. J., 240 (2014) 271–280.

[34] S. Karanjit, A. Jinasan, E. Samsook, R.N. Dhital, K. Motomiya, Y. Sato, H. Sakurai, Significant stabilization of palladium by gold in the bimetallic nanocatalyst leading to an enhanced activity in the hydrodechlorination of aryl chlorides, Chem. Commun., 51 (2015) 12724–12727.

[35] J. Zhou, H. Chen, Q. Chen, Z. Huang, Bimetallic Au-decorated Pd catalyst for the liquid phase hydrodechlorination of 2,4-dichlorophenol, Appl. Surf. Sci., 387 (2016) 588–594.

[36] O.S.G. Soares, J.J. Órfão, M.F.R. Pereira, Bimetallic catalysts supported on activated carbon for the nitrate reduction in water: optimization of catalysts composition, Appl. Catal., B, 91 (2009) 441–448.

[37] L. Chen, W. Kong, J. Yao, H. Zhang, B. Gao, Y. Li, C. Jiang, Synthesis and characterization of Mn-Co-Ni-O ceramic nanoparticles by reverse microemulsion method, Ceram. Int., 41 (2015) 2847–2851.

[38] Z. Yan, M. Wang, Y. Lu, R. Liu, J. Zhao, Ethylene glycol stabilized NaBH₄ reduction for preparation carbon-supported Pt–Co alloy nanoparticles used as oxygen reduction electrocatalysts for microbial fuel cells, J. Solid State Chem., 18 (2014) 1087–1097.

[39] M.A. Alvarez-Montero, L.M. Gómez-Sainero, J. Juan-Juan, A. Linares-Solano, J.J. Rodriguez, Gas-phase hydrodechlorination of dichloromethane with activated carbon-supported metallic catalysts, Chem. Eng. J., 162 (2010) 599–608.

[40] R.L. Frost, Y. Xi, B.J. Wood, Thermogravimetric analysis, PXRD, EDX and XPS study of chrysocolla (Cu,Al)₂H₂Si₂O₅(OH)4·nH₂O-structural implications, Thermochim. Acta, 545 (2012) 157–162.
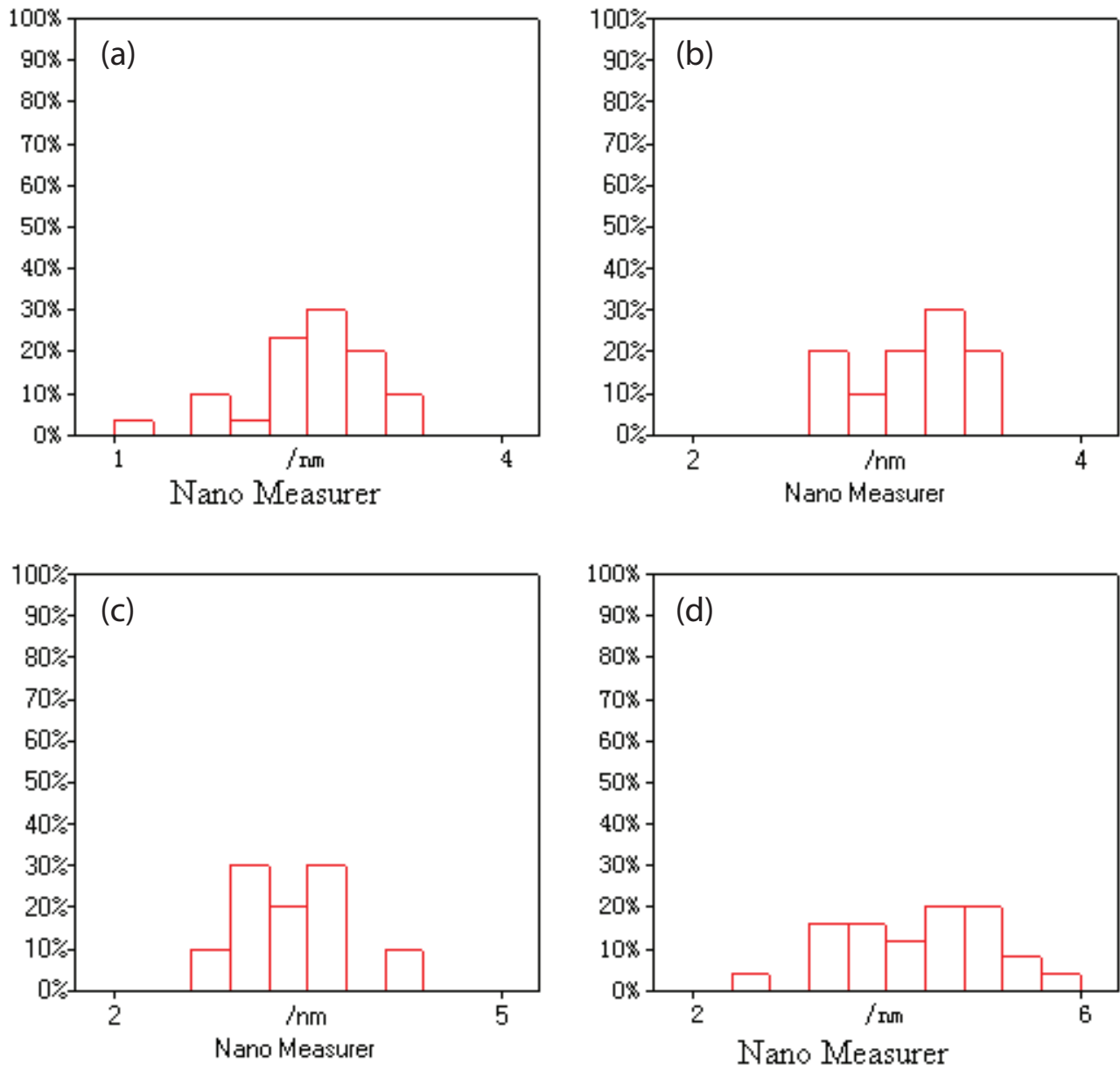
Supplementary material

Fig. S1. (a) CuPd-0.3/1 particle size distribution; (b) CuPd-0.5/1 particle size distribution; (c) CuPd-1/1 particle size distribution; and (d) CuPd-3/1 particle size distribution.
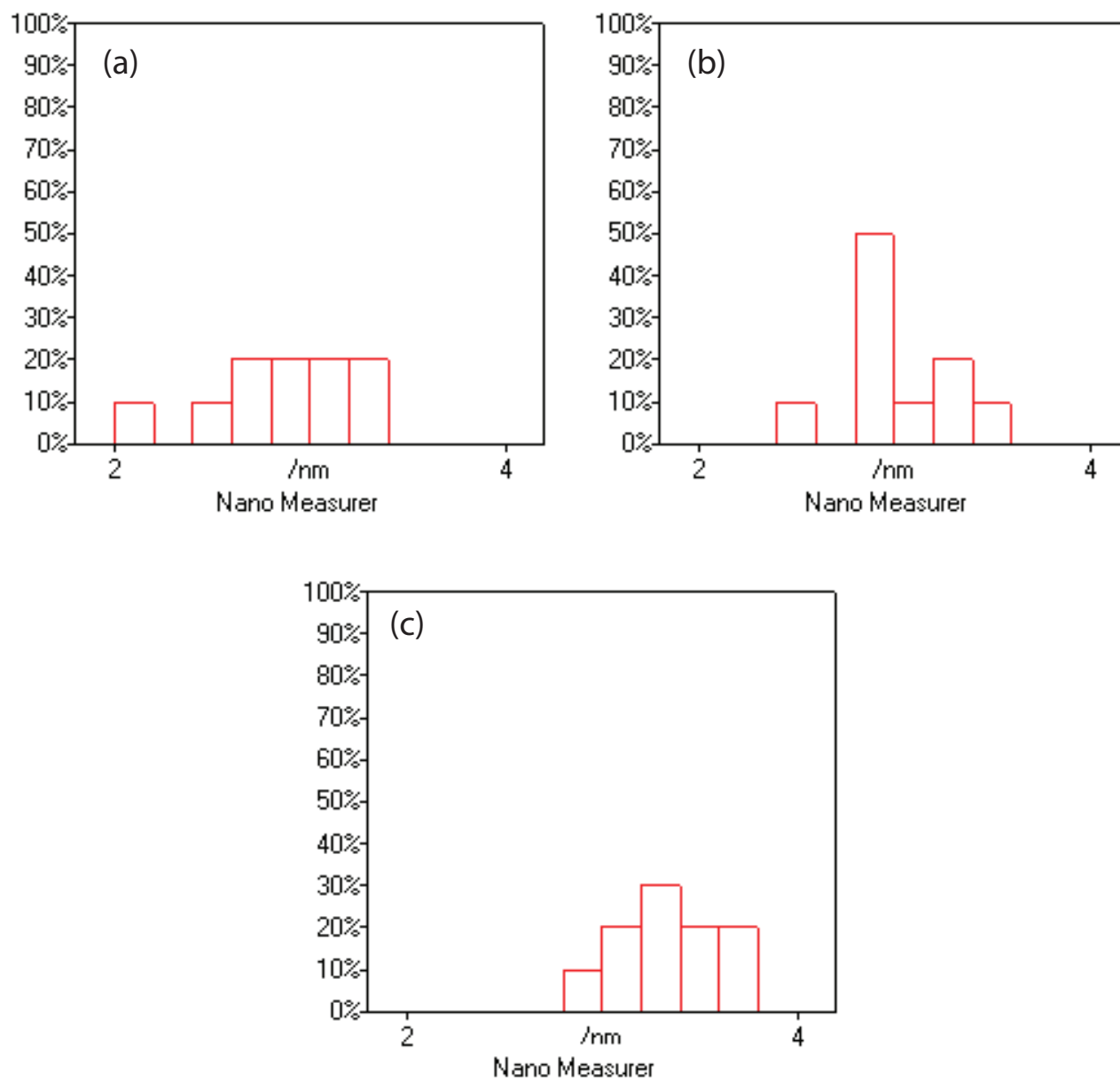
Fig. S2. (a) CuPd(me)-0.5/1 particle size distribution; (b) CuPd(me)-1/1 particle size distribution; and (c) CuPd(me)-3/1 particle size distribution.